Atomic Auger decay in core-excited HBr by angle-resolved two-dimensional photoelectron spectroscopy

Ximao Feng,[1,*] Antony A. Wills,[1] Emma Sokell,[2] Marco Wiedenhoeft,[1] and Nora Berrah[1]
[1]*Department of Physics, Western Michigan University, Kalamazoo, Michigan 49008, USA*
[2]*School of Physics, University College Dublin, Republic of Ireland*
(Received 14 October 2006; published 24 January 2006)

Angle-resolved two-dimensional photoelectron spectroscopy has been used to study HBr in the vicinity of the Br 3*d* ionization thresholds. The energy positions of the two $3d_{5/2,3/2} \rightarrow \sigma^*$ resonances have been measured directly and found to be at 70.89(6) eV and 71.92(6) eV, respectively, giving a spin-orbit splitting of 1.03(3) eV for the two Br 3*d* components. Br Auger lines (26 eV < KE < 54 eV), produced by dissociation of HBr after $3d \rightarrow \sigma^*$ transitions, are tentatively assigned according to their kinetic-energy positions and their profiles as a function of photon energy are found to be asymmetric. The angular distribution asymmetry parameters β of these lines, which have not been measured before, have also been derived. The alignment parameters for the two intermediate atomic states ($^2D_{5/2}$ and $^2D_{3/2}$) have been found and used to derive intrinsic anisotropy parameters α_2 from the β parameters. These were found to be similar to those of the equivalent $M_{4,5}NN$ normal Auger lines in the isoelectronic counterpart Kr calculated by Tulkki *et al.* [Phys. Rev. A **48**, 1277 (1993)].

DOI: 10.1103/PhysRevA.73.012716 PACS number(s): 32.80.Hd, 32.80.Fb, 31.70.Hq, 31.15.Gy

I. INTRODUCTION

When an inner-shell electron is excited to an antibonding orbital in a molecule, the molecule starts to dissociate. If the core-hole lifetime of the parent molecule is comparable to the dissociation rate, both sharp atomic Auger decay lines and broad molecular Auger decay lines can be present in the resonant Auger electron spectrum. The atomic decay occurs within an excited atom after the dissociation is complete, while the molecular decay takes place at small internuclear distances where the interaction between the fragments cannot be neglected. Morin and Nenner [1] were the first to observe the sharp atomic decay lines after core excitation in HBr. Following this pioneering work, other small molecules, including HF [2], HCl [3–15], HBr [16], NH_3 [17], PH_3 [18,19], H_2O [20], and H_2S [21,22], have also been used to study the competition between the atomic and molecular Auger decay. Improved photoelectron spectroscopy techniques have been extensively used to reexamine the case of HCl [3–15], but not HBr.

In this work, we present an extensive two-dimensional photoelectron spectrum (2DPES) of HBr. The electronic configuration of HBr in its ground state is $1s^2 2s^2 2p^6 3s^2 3p^6 3d^{10} 4s\sigma^2 4p\sigma^2 4p\pi^4$, and its next higher empty orbital is $4p\sigma^*$. The 2DPES spans a photon energy range of 10 eV, covering the following three regions: (1) 3*d* excitation to the unoccupied, $4p\sigma^*$ molecular orbital, (2) 3*d* excitation to Rydberg orbitals, and (3) 3*d* ionization. The analysis of the 2DPES has focused in particular on the atomic decay channel following the $3d \rightarrow \sigma^*$ transition. We have resolved the $3d_{5/2,3/2} \rightarrow \sigma^*$ resonances by observing selective decay to the accessible final states. We have also investigated the profile of the atomic Auger emission as a function of photon energy. We have measured the angular distribution parameters β of the atomic lines, and from their β values, we have derived their intrinsic anisotropy parameters α_2 and compared them with those of the corresponding $M_{4,5}NN$ normal Auger lines in the isoelectronic counterpart, Kr.

II. EXPERIMENTAL METHOD

The experiment used monochromatized synchrotron radiation from the undulator beamline 10.0.1 at the Advanced Light Source (ALS) at Lawrence Berkeley National Laboratory in tandem with a time-of-flight (TOF) electron spectrometer system [23,24]. Details of the experimental setup used to perform the angle-resolved, two-dimensional photoelectron spectroscopic studies have been given elsewhere [24,25]. Briefly, the system consists of two time-of-flight electron-energy analyzers mounted 125.3° apart in a rotatable chamber in a plane perpendicular to the direction of the photon-beam propagation. HBr gas was leaked into the chamber from a 0.5-mm-inner-diameter gas needle which was equidistant from the two analyzers. Electron TOF spectra were measured simultaneously at 0° and 54.7° relative to the polarization plane of the incident radiation. After rotation of the chamber, spectra at another set of angles, 35.3° and 90°, were recorded. The HBr pressure was maintained at about 2×10^{-5} Torr in the chamber. The TOF resolution is estimated to be about 1% of the kinetic energy of the electrons. To increase the resolution of the spectra within the measured areas of interest, a 20-eV retarding potential was applied to each TOF tube. The resolution of the photon beam was set at approximately 80 meV in the photon energy range of interest. The degree of the linear polarization was approximately 0.99 [26,27].

To build up the two-dimensional photoelectron spectra or *maps*, we first collected two one-dimensional photoelectron

*Electronic address: ximao.feng@wmich.edu

spectrum, or slices, at the lowest photon energy of interest for 20 s; then, we incremented the photon energy by 20 meV and collected another pair of 1DPES. This process was repeated until the photon energy range of interest was covered and hence two 2DPES were obtained at angles that were 125.3° apart. To obtain better statistics, we collected six sets of 2DPES at each angle under the same experimental conditions. Five of them had the same photon-energy range, while the sixth covered higher energies. The final 2DPES was obtained by aligning all six data sets on the time and photon energy scales and averaging the electron intensity at each data point. The original 2D map was then converted from an electron time-of-flight scale to a kinetic-energy scale [28]. The time–to–kinetic-energy conversion points were obtained from the $2s$ and $2p$ lines of Ne [29], whose 2DPES was collected under similar experimental conditions as HBr. The kinetic-energy step size was 20 meV and the systematic error in the time–to–kinetic-energy conversion is ±30 meV. Since the Ne $2s$ intensity is zero at 90°, the time–to–kinetic-energy conversion points for the HBr data recorded at 90° were obtained from the HBr data taken at the magic angle which had been converted to the kinetic-energy scale. The photon-energy scale was calibrated using the energies of HBr resonances [30]. All the spectra in the 2DPES have been corrected for variations in the incident photon flux. The transmission efficiency for each of the TOF analyzers and their relative detection efficiencies were obtained using the $2s$ and $2p$ lines of Ne, whose cross sections [31] and angular distribution parameters [32] are well known. To calibrate the HBr data at 90°, we used Ne data recorded at 75°. This angle was chosen as a compromise between sufficiently strong Ne $2s$ intensity and an angle as close to 90° as possible. Though the transmission functions at these two angles are expected to be similar, use of the 90° data has accordingly larger uncertainties than use of data of other angles.

III. RESULTS AND DISCUSSION

A. Two-dimensional photoelectron spectrum for 3*d* excitation in HBr

The 2DPES *map* of HBr in the vicinity of the $3d$ ionization thresholds is shown in Fig. 1. This 2DPES is similar to previous work in Ne [33], Ar [34], Kr [35], Xe [36], and HCl and DCl [37]. In the 2DPES, electron intensities are plotted as a function of electron kinetic energy and photon energy. Different intensities are represented by different colors, as shown by the color bar at the lower-right corner of Fig. 1. Intensities below a lower cutoff threshold are shown as white while those above an upper cutoff threshold are shown as black.

The main panel of the 2DPES shows the Auger and photoelectrons emitted in three photon-energy regions corresponding to three distinct processes: the resonant $3d_{5/2,3/2} \rightarrow \sigma^*$ and $3d_{5/2,3/2} \rightarrow nl\lambda$ excitations and ionization and $3d_{5/2,3/2} \rightarrow \epsilon l$. These regions are marked in the right panel where the summed electron yield in the 2D map is extracted and displayed as a function of photon energy. The horizontal arrows show the positions of the two $3d_{5/2,3/2} \rightarrow \sigma^*$ ($^2D_{5/2}$ and $^2D_{3/2}$) resonances. The two one-dimensional photoelectron spectra (1DPES) shown in the bottom panels were extracted from the 2DPES at the photon energies of these two resonances, indicated by the arrows at the sides of the 2DPES. Another 1DPES corresponding to the last slice ($h\nu$=78.7 eV) of the 2DPES is also shown in the top panel. The narrow *prompt*, indicated by the vertical arrows on the top panel and the panel below the main panel, corresponds to photons that essentially arrive instantaneously at the detectors of the TOF analyzers.

We identify four types of features in this 2DPES map.

(1) Three continuous and strong diagonal lines with a slope of unity. They are the three valence photolines: namely, $4p\pi^{-1}$, $4p\sigma^{-1}$ and "$4s\sigma^{-1}$." The quotation marks indicate the main line of the $4s\sigma^{-1}$ state. Around the main line, there are at least seven parallel ones of lower intensity which are the satellite lines of the $4s\sigma^{-1}$ state [38]. Incidentally, the two photolines evident in the lower-right corner of the main panel correspond to $3d$ photoionization by photons produced by the second harmonic of the undulator—i.e., $2\times h\nu$. This has a slope of twice that for the valence photolines produced with the main first-order harmonic.

(2) Many narrow vertical lines superimposed on a continuous background in the photon energy range 69.5 eV and 73.5 eV. These atomic Auger lines [1,16], produced when excited $Br^*(3d^{-1}4p^6)$ atoms emit electrons after dissociation of the HBr molecules, fall into two groups according to their maxima on the photon energy scale. Since the kinetic energy of these Auger electrons depends only on the energy difference between the initial excited Br^* state and the singly charged Br^+-ion state, the atomic lines appear on the 2DPES map as vertical lines (constant kinetic energy). One group of lines has a maximum at 70.9 eV and the other at 71.9 eV (indicated by horizontal arrows in Fig. 1) which correspond to the two $3d_{5/2,3/2} \rightarrow \sigma^*$ resonances. The background underlying these atomic Auger lines is formed by electrons emitted before dissociation is complete.

(3) Horizontal lines above 73.5 eV arise from molecular Auger decay following excitation of various $3d$ Rydberg resonances [30,39–41]. A particular resonance may decay to different final states. All of these Auger electrons occur at the photon energy of a Rydberg resonance, and hence these features appear as horizontal lines in the 2DPES.

(4) Vertical lines above the photon energy of 77 eV, which correspond to normal Auger decay following the photoionization of $3d$ electrons [42–44]. For a given Auger transition the electrons have a constant kinetic energy, the energy difference between the intermediate core-hole state and the doubly charged final-state HBr^{++}. However, as the $3d$ ionization thresholds are approached from above these lines shift towards higher kinetic energies, demonstrating the effect of postcollision interaction.

B. Kinetic energies and assignments of the atomic Auger lines

The atomic Auger decay lines are shown in detail in Fig. 2. The 2DPES map was recorded at 90° with respect to the polarization of the photon beam. The $4s\sigma^{-1}$ and $4p\sigma^{-1}$ photolines are weak at this angle, indicating that they have positive angular distribution parameters. Therefore, this 2DPES

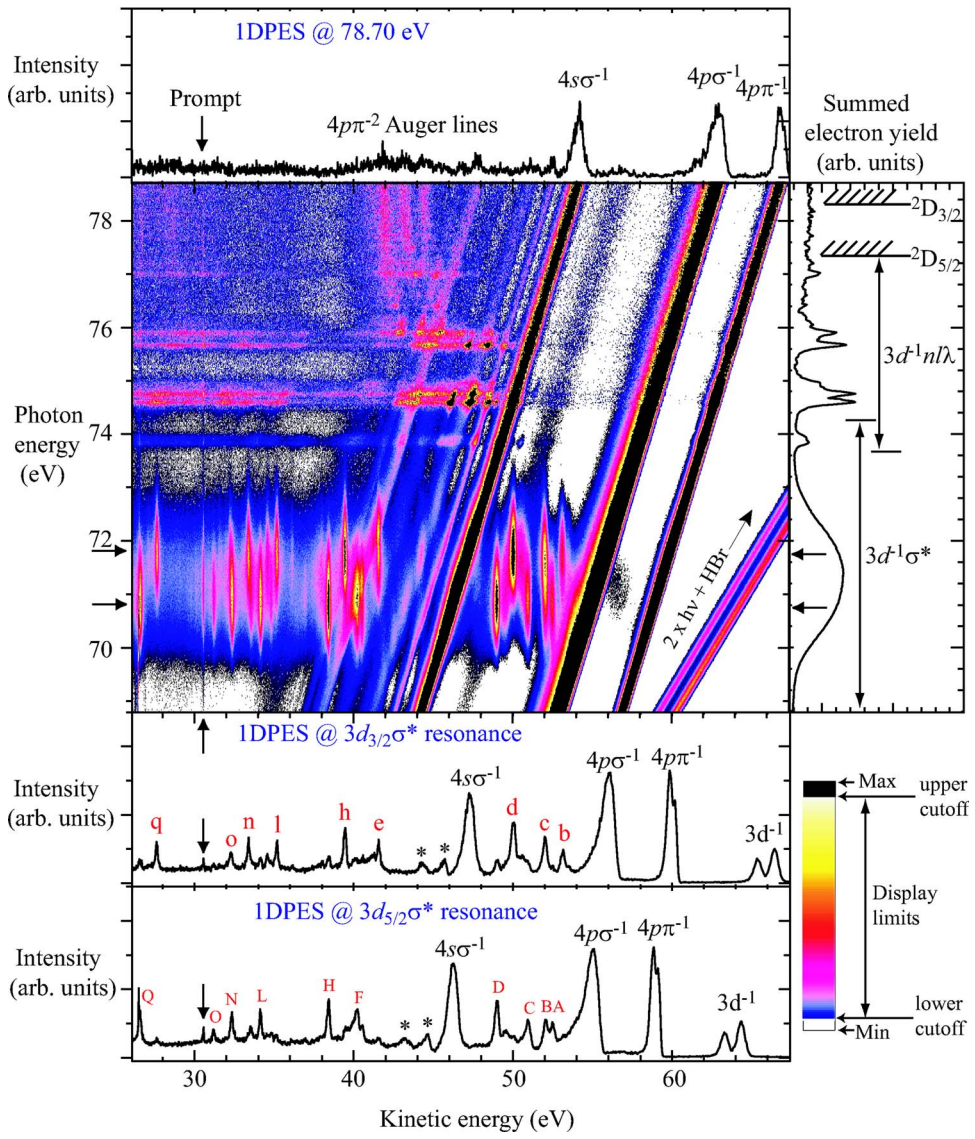

FIG. 1. (Color online) Two-dimensional photoelectron spectrum (2DPES) of HBr including all $3d$ resonances and the $3d_{5/2,3/2}$ ionization thresholds. The spectrum shown was taken at 0° relative to the electric field vector of the photon beam. Different electron intensities are represented using different colors as shown by the color bar in the lower-right corner. In the right panel, the pseudoabsorption spectrum formed by summing all of the electron yield in the 2DPES as a function of the photon energy is shown. Three conventional one-dimensional photoelectron spectra extracted from the 2DPES are shown: the top panel corresponding to the last photon energy value (78.70 eV) of the 2DPES and the two panels below the 2DPES corresponding to the spectra on the $3d_{5/2,3/2} \rightarrow \sigma^*$ resonances, whose energy positions are shown with horizontal arrows on both sides of the main panels. In the 1DPES spectra at the $3d_{5/2,3/2} \rightarrow \sigma^*$ resonances, the three valence photolines ($4p\pi^{-1}$, $4p\sigma^{-1}$, and "$4s\sigma^{-1}$"), the $3d^{-1}$ photoline formed with second-order radiation, the most intense resonant Auger lines (letters), and two satellite lines (stars) of the $4s\sigma^{-1}$ state are shown. The narrow prompt evident in each 2DPES corresponds to photons that essentially arrive instantaneously at the detectors in the TOF analyzers. For a detailed explanation of the 2DPES see the main text.

allows the atomic lines in the vicinity to appear most clearly. Each atomic Auger decay line can be seen across a broad photon energy range of more than 3 eV.

There are 16 atomic lines evident in the 2DPES that have their maxima at 70.89 eV on the photon energy scale; these are produced from the $3d_{5/2} \rightarrow \sigma^*$ resonance. At the $3d_{3/2} \rightarrow \sigma^*$ resonance, around 71.92 eV, 15 lines are observed. In the absence of any selection rules it would be reasonable to assume that there should be an equal number of lines from the two resonances. However, the differing values of the total angular momentum in the two resonance states means that the angular momentum carried away by the Auger electron may be different for the $3d_{5/2} \rightarrow \sigma^*$ and $3d_{3/2} \rightarrow \sigma^*$ transitions. This could result in the suppression of certain atomic lines in one resonant Auger spectrum when it is compared with the other. For completeness, all the missing lines, whose positions have been derived from the other resonance, are marked in Fig. 2 with dashed lines. The lines associated with the $3d_{5/2} \rightarrow \sigma^*$ resonance are labeled with uppercase letters from A to Q and those associated with the $3d_{3/2} \rightarrow \sigma^*$ resonance with lowercase letters from a to q. Their kinetic-energy positions are listed in Table I as col-

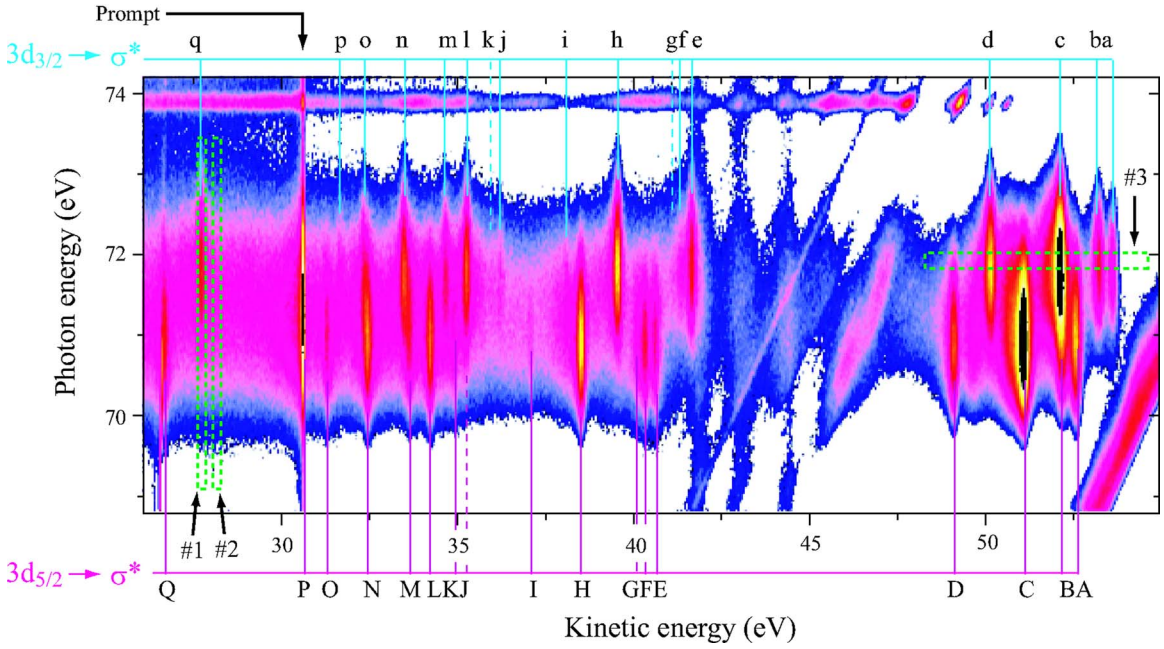

FIG. 2. (Color online) Detailed map of the atomic Auger lines decaying from the initial $Br^*(3d^{-1}_{5/2,3/2}4p^6)$ state after dissociation of the core-excited HBr^* $(3d_{5/2,3/2} \rightarrow \sigma^*)$. This map was measured at 90° with respect to the electric field vector of the photon beam. For best visual effect, the data have been nine-point smoothed and the intensities shown are the square roots of the smoothed values.

umns 3 ($^2D_{5/2}$) and 12 ($^2D_{3/2}$). The errors in the brackets include a systematic error of 30 meV and relative errors.

Two lines which have the same final ionic state but which originate from each of the two σ^* resonances will be termed an *atomic line pair* in this work. One member of the pair is labeled with an uppercase letter and the other with the same lowercase one. Their separation on the kinetic-energy scale, approximately 1.03 eV, corresponds to the spin-orbit splitting of Br 3*d*.

The line assignments, listed in the first column of Table I, were obtained by comparing the kinetic energies of the lines in our 2DPES with Br^+ optical energy levels given in Ref. [45], equivalent lower-resolution spectra [1], Br^+ energy levels following the $3d^{-1}4p^6\ ^2D_{5/2}$ transition in atomic bromine [46] (column 7 in Table I), and with Kr Auger spectra [47,48]. In the latter two Kr spectra the decay lines have the equivalent initial and final states as the corresponding resonant Auger decay lines in the bromine atom.

Lines *A*–*H* were the first fragment Auger lines identified [1], and our energies are consistent with those given by these authors. However, these energies appear to be systematically lower than those given by Ref. [16] (columns 5 and 13). One advantage of recording a single 2DPES is that the energies of all lines, specifically those originating with different resonances, will be affected equally by any systematic errors, as long as the kinetic-energy scale is linear. This does not appear to be the case for the 1DPES recorded by Liu *et al.* [16]. The energies of the Auger peaks resulting from decays filling the $3d_{5/2}$ hole are 100 meV higer than the values obtained in the present work, while those resulting from decays filling the $3d_{3/2}$ hole are 200 meV higher. Despite these discrepancies the identification of the *atomic line pairs A–H* is unambiguous. This is not the case for the pairs with lower kinetic energies with the exception of pair *Q* which has been assigned in accordance with Ref. [46] and by comparison with Kr spectra [48]. The remaining assignments in the table were obtained using the optical data of Ref. [45]. These binding energies were converted to kinetic energies using the $4s^24p^4\ ^3P_2$ line at52.48 eV as a reference and are listed as column 6. Optical lines whose energy values are within the error range of our corresponding line position have been used to determine possible assignments for these lines.

There is no evidence in the 2DPES for the line *g* $(4s^14p^5\ ^3P_0)$, in agreement with the discovery from the Kr Auger spectrum [47]. Lines *L* and *l*, the two most intense ones between 30 eV and 37 eV, have not be assigned because there are no reference lines within ±200 meV of their kinetic-energy positions. Jauhiainen *et al.* [48] made a similar observation when they tried to assign the equivalent lines in their krypton spectrum using the optical energy levels given by Moore [49]. Those authors concluded that some of the reference optical levels are given incorrect assignments, a conclusion borne out by McGuire [50]. Consequently, the assignments of line pairs *I*–*P* remain tentative. In particular, the correspondence between the peaks identified by Nahon *et al.* [46] and those listed in Table I is not definite.

C. Asymmetric profile of the atomic Auger lines on the photon-energy scale and energy positions of the $3d_{3/2,5/2} \rightarrow \sigma^*$ resonances

The dependence of the dissociation rate on photon energy has been studied in HBr by Liu *et al.* [16] and in HCl by Kukk *et al.* [9] and Björneholm *et al.* [8]. These studies were done by comparing the relative contributions from atomic and molecular decays. In the HBr work, the authors found that the atomic decay contribution increases relative to the molecular components as the photon energy increases. For

TABLE I. Assignments, kinetic energies, intensities (measured at the magic angle), and angular anisotropy parameters β of the atomic Auger lines resulting from dissociation following $3d \rightarrow \sigma^*$ transitions in HBr. Some references are also shown for comparison.

	$3d_{5/2}$ decay (hν=70.89 eV)									$3d_{3/2}$ decay (hν=71.92 eV)				
	Peak	Energy (eV)					Intensity			Peak	Energy (eV)		Intensity	
Final state	label	this work	Ref.[1]	Ref.[16]	Ref.[45]	Ref.[46][a]	this work	Ref.[46]	β	label	this work	Ref.[16]	this work	β
$4s^2 4p^4(^3P_2)$	A	52.48(5)		52.58	52.48		95(9)		0.0(1)	a	53.50(5)	53.70	35(4)	0.0(1)
$(^3P_1)$	B	52.04(4)	52.2	52.16[b]	52.09	52.54	56(8)	175	0.31(8)	b	53.08(5)	53.30[c]	60(6)	0.30(6)
$(^3P_0)$					52.00									
$(^1D_2)$	C	50.97(4)	50.8	51.08	50.98	51.15	135(4)	163	-0.45(16)	c	52.01(5)	52.19	130(6)	-0.41(6)
$(^1S_0)$	D	49.00(4)	49.0	49.09	49.02	49.22	85(5)	108	0.65(15)	d	50.02(5)	50.21	98(5)	0.59(13)
$4s^1 4p^5(^3P_2)$	E	40.53(4)			40.52		38(5)		0.40(5)	e	41.57(4)		59(5)	0.37(5)
$(^3P_1)$	F	40.24(5)	40.2		40.23	40.35	49(10)	103	0.50(16)	f	41.23(5)		17(9)	0.30(14)
$(^3P_0)$	G	40.05(5)			40.05		25(10)		0.66(25)	g	-		-	-
$(^1P_1)$[e]	H	38.42(4)	38.4		38.43	38.45	98(5)	98	0.29(6)	h	39.47(4)		98(5)	0.22(6)
$4s^2 4p^3(^2P^0)5s(^1P_1)$	I	36.95(5)			36.98		9(2)		0.4(2)	i	37.98(5)		7(2)	0.43(14)
$4s^2 4p^3(^4S^0)5d(^3D)$	J	35.08[d]			35.11–21		-		-	j	36.11(5)		7(2)	0.3(2)
(^5D)					35.06–10									
$4s^2 4p^3(^2P^0)5p(^3D)$	K	34.83(4)			34.66–86		22(9)		0.5(2)	k	-		-	-
?	L	34.14(4)				34.06	71(4)	156	0.31(8)	l	35.17(4)		57(5)	0.25(6)
$4s^2 4p^3(^2D^0)5d(^1D)$	M	33.53(4)			33.53		21(5)		0.2(1)	m	34.57(4)		25(3)	0.28(10)
$4s^2 4p^3(^2D^0)4f(^1D)$[e]					32.41									
(^3F)[e]	N	32.35(4)			32.36–7	32.24	55(5)	85	0.30(9)	n	33.38(4)		50(5)	0.21(5)
(^3D)[e]					32.35-50									
(^1F)[e]					32.35									
?	O	31.19(4)				30.99	26(3)	47	0.31(5)	o	32.22(4)		23(3)	0.26(5)
?	P	30.53(5)				-	-		-	p	31.57(5)		-	-
$4s^0 4p^6(^1S_0)$	Q	26.58(4)				26.33	64(3)	127	0.75(8)	q	27.62(4)		59(2)	0.60(5)

[a]Converted from binding energy at the photon energy of 64.54 eV given by the authors.
[b]Misprinted as 51.16 in [16].
[c]Misprinted as 52.30 in [16].
[d]Derived from the position of the other spin-orbit component.
[e]Different from the assignment given by Ref. [46].

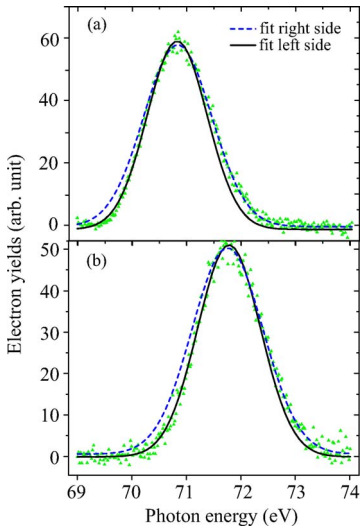

FIG. 3. (Color online) Asymmetry observed in the atomic Auger spectrum as a function of photon energy of atomic lines (a) H at 90° and (b) q at 0°. In each panel, the experimental intensity, represented by solid triangles, is only the atomic contribution without the molecular background. Two Gaussian fits are shown for different photon-energy ranges of each line: left half (solid line) and right half (dashed line). (See text for details.)

HCl, Kukk *et al.* found that at the low-photon-energy side of the resonance, molecular Auger decay dominates over the atomic Auger decay [9]. With increasing photon energy, the dominance is gradually transferred from the molecular decay to the atomic decay. However, other workers [8] found experimental evidence showing that the molecular decay fraction has a minimum on top of the resonance and increases as the detuning increases in both negative and positive directions.

In this work, we focus on determining the asymmetric nature of the measured atomic lines on the photon-energy scale. This asymmetry arises from the shape of the potential-energy curve of the intermediate resonance state. The extraction of net excitation function, the atomic contribution as a function of photon energy, of one line is shown in Fig. 2 with line q as an example. The dashed box No. 1 drawn vertically around line q in Fig. 2 shows the area into which most of the electron yield of this line falls. Its total intensity as a function of photon energy was obtained by projecting all of the electron yield within the rectangle onto the photon-energy axis. Similarly, the molecular background can be obtained from the box No. 2 immediately to the right of the total intensity box. The difference of the total intensity and backgound is the net atomic excitation function of line q. Usually the sharp atomic Auger lines have a broad molecular background at the low-kinetic-energy side [10,14]. Consequently, it is reasonable to determine the background from the right, high-kinetic-energy, side of the atomic line.

The net excitation functions of atomic lines H (top panel) at 90° and q (bottom panel) at 0° are shown as scattered triangles in Fig. 3. These two lines have been selected as they are well separated from their neighbors and have a low constant molecular background. This simplifies the determination of the net excitation function which only contains atomic contributions. Peak H corresponds to the decay $\mathrm{Br}^*(3d_{5/2}^{-1}4p^6) \rightarrow \mathrm{Br}^+(3s^1 3p^5\ ^1P_1) + e^-$ and line q to the decay of $\mathrm{Br}^*(3d_{3/2}^{-1}4p^6) \rightarrow \mathrm{Br}^+(3s^0 3p^6\ ^1S_0) + e^-$. For both lines, the intensity at 0° is larger than at any other angle. However, at this angle, the $4s\sigma^{-1}$ satellite lines, which run under line H, are also at their strongest. Thus, the data recorded at 90° are used for line H; at this angle, the photoline background can be neglected.

To illustrate the asymmetric nature of the profiles, we fitted the net electron intensity of each line with two Gaussian profiles, each time fitting only a part of the spectrum. For example, for line q, whose maximum is around 71.9 eV, the low-energy section between 69.0 eV and 72.2 eV was first fitted (solid curve) and, then, the high-energy side between 71.6 eV and 74 eV (dashed curve) was fitted. The fitting shows that these two atomic lines are asymmetric: the Gaussian-fit curves for the high-energy side clearly have higher intensities and larger widths than the experimental curves on the low-energy side. On the other hand, the fit curves for the low-energy side show lower intensities and smaller widths than the experimental ones on the high-energy side. This indicates clearly that the atomic decay lines on the photon-energy scale are asymmetric with a higher tail at the high-energy side, suggesting that the atomic contribution becomes more significant with increasing photon energy. The asymmetry is related to the profile of the potential-energy curve of the excited state. The wave function of the HBr molecule in its vibrational ground state can be approximated by that of an harmonic oscillator, which has a Gaussian profile with a maximum at the equilibrium internuclear separation. The projection of this distribution onto the dissociative curve of the $4p\sigma^*$ state may result in an asymmetric absorption spectrum. Furthermore, the dissociation rate increases with photon energy and consequently the atomic lines exhibit asymmetric profiles along the photon energy axis.

This fitting process also provides the energy positions of the two σ^* resonances for the first time. Previous studies on core-excited HBr molecules, either with energy-loss spectroscopy [51] or photoabsorption spectroscopy [40], only presented the total contribution from the two $3d_{5/2,3/2} \rightarrow \sigma^*$ resonances without being able to separate them because of their broad linewidths. Photons having an energy corresponding to the separation between this potential energy curve of the ground state and that of the resonance state at the internuclear separation, R_e, can excite the most molecules. Provided that any variation in the dissociation rate is less significant than the variation in the probability distribution of the ground-state molecules, maxima in the atomic Auger line profiles on the photon-energy scale are also the resonant-energy positions. From the above fits to lines H and q and additional checking with other atomic lines, we obtain the resonance positions at 70.89(6) eV ($^2D_{5/2}$ resonance) and 71.92(6) eV ($^2D_{3/2}$ resonance), and their common width is found to be 1.25(6) eV. The determination of the two resonance positions is expected to be helpful in calculating the potential-energy curves of the intermediate states.

The energy difference of the two resonances, 1.03(3) eV, is the spin-orbit splitting of Br $3d$ which is in agreement with

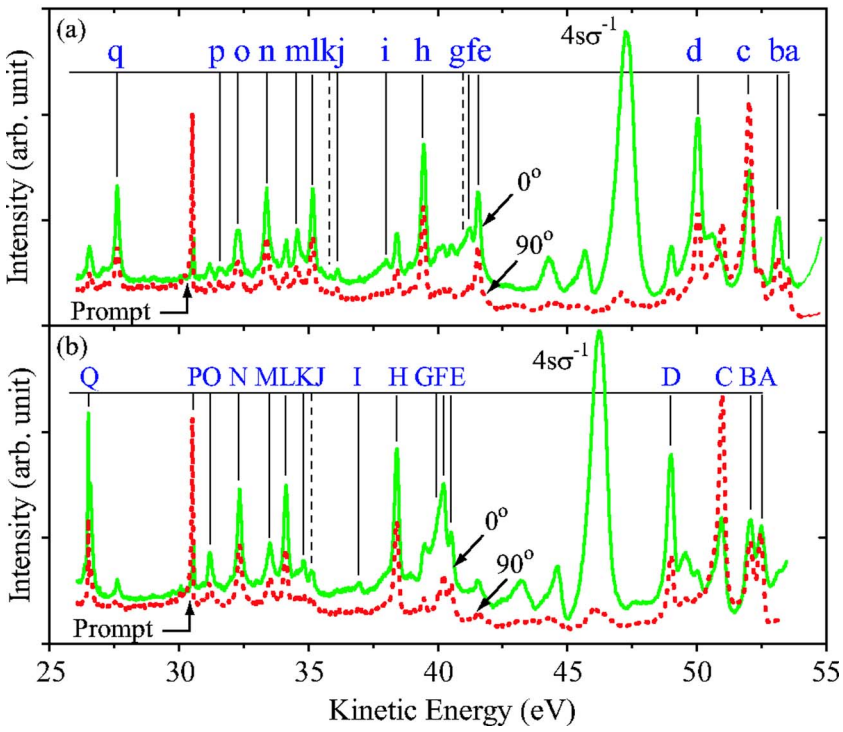

FIG. 4. (Color online) Resonant PES spectra at 0° (solid lines) and 90° (dashed lines) for the $3d_{3/2} \rightarrow \sigma^*$ (a) and $3d_{5/2} \rightarrow \sigma^*$ (b) resonance states.

the splitting obtained from the kinetic-energy positions of the atomic lines. This splitting value is similar to those obtained from other Br containing molecules, such as 1.04 eV given by Hitchcock and Brion [52] from CH_3Br and Hitchcock *et al.* [53] from C_6H_5Br, and 1.020(6) eV found by Shaw *et al.* [51] from Br_2. It is also in reasonable agreement with 1.11(1) eV determined by Shaw *et al.* [51] from the 3*d* Rydberg resonances in HBr.

D. Intensity and angular distribution of the atomic lines

Molecular Auger decay usually shows little or no anisotropy. However, Becker and Menzel [5] and Kukk *et al.* [9] found surprisingly large anisotropy in the Cl^* atomic decay following dissociation of core-excited HCl molecules. In the following section, we show that this is also the case for core-excited HBr molecules.

In the dipole approximation, the angular distribution of the emitted atomic Auger electrons produced from the fragments can be written as [54]

$$W(\theta) = (W^{(T)}/4\pi)[1 + \beta P_2(\cos\theta)], \qquad (1)$$

where $W(\theta)$ is the differential cross section, $W^{(T)}$ is the total cross section, θ is the angle between the direction of the electron emission and the electric field vector of the polarized photon beam, β is the asymmetry parameter, and $P_2(\cos\theta)$ is the second-order Legendre polynomial.

If the Auger decay occurs before the molecule has fragmented, the angular asymmetry is simply the product of the molecular alignment parameter, describing the orientation of the molecules with respect to the electric field vector, and the intrinsic anisotropy parameter for the Auger decay, α_2 [10]. For the two-step atomic decay process, the angular asymmetry is the product of the alignment parameter for the intermediate atomic state and α_2. However, depending on the competition between dissociation and Auger decay, electron emission will occur at all internuclear separations between that of the resonance state when it is first excited and the separated atom limited (in this picture any vibrational motion has been ignored). Indeed, if the two potential energy curves become parallel before the molecule has completely fragmented, molecular decays will contribute to the atomic peak. It is interesting then that molecular Auger emission shows little anisotropy while atomic Auger emission tends to exhibit a large amount. Data from the two-dimensional map can be used to investigate this process in more detail. Figure 4 presents Auger electron spectra extracted from the 2DPES recorded at 0° and at 90° in the vicinity of the $3d_{3/2} \rightarrow \sigma^*$ (a) and $3d_{5/2} \rightarrow \sigma^*$ (b) resonance states. From the figure, one can see clearly that the $4s\sigma^{-1}$ main line shows a strongly positive angular anisotropy as expected. More interesting is the apparent intensity variations for some of the atomic Auger lines. While lines *c* and *C* have higher intensities at 90° than at 0°, lines *d*,*D*, *q*, and *Q* are more intense at 0°. Any angular anisotropy suggests that the decays contributing to the atomic peak occur when the molecule has fragmented completely rather than in the molecular regime where the potential-energy curves have become parallel.

Strictly speaking, *atomic* and *molecular* Auger decay contributions to PES are not separable since an Auger decay may occur throughout a continuous range of internuclear distances from the region of the initial excitation all the way to the separated atom limit. The sharp *atomic* part of the Auger-electron-energy distribution may well result from tranisitions between two nearly parallel potential-energy curves before the dissociation limit is actually reached. This being said, it can still be instructive to extract intensities for the sharp peaks alone, as previous authors have done in HCl–for example [10]—and to compare the results to Kr Auger decay

data in order to investigate their general atomiclike character.

The remaining discussions of this paper will all be concerned with the data extracted to represent the *atomic* contributions. To extract the intensities of the atomic contribution as accurately as possible, we have used four methods.

(1) Extracting the total intensity as a function of photon energy and fitting it with Gaussian functions. This method was used for lines without strong background, such as *A*, *B*, *a* and *b*. In this case the total and net (atomic contribution) intensities are not significantly different.

(2) Obtaining the net excitation function by subtracting the molecular background from the total intensity. This method is suitable for lines well separated from any other lines. In this case, the molecular backgrounds to the right of the line in the 2DPES are treated as approximately constant. This method was employed in determining the atomic contribution for lines *q* and *H*.

(3) Gaussian fit of the lines in the 1DPES. This method does not give accurate results for weak peaks. Extraction of a conventional 1DPES from the 2D map, in the region of the lines *a–d*, can be achived by projecting all of the electron yield within the box No. 3, drawn horizontally on top of lines *a–d* in Fig. 2 onto the kinetic-energy axis.

(4) Determining the net peak intensity from the 1DPES by subtracting a linear background. Because of the difficulties associated with determining the background, this method was generally only used as a check of the other methods. However, two lines *I* and *j* were too weak to employ any other method.

The normalized intensities of the atomic lines are listed as columns four ($^2D_{5/2}$ resonance) and nine ($^2D_{3/2}$ resonance) in Table I. The final value for each line is the average of all the results derived with one or more of the above methods. The variations among different values were used to determine the error. To compare with the relative intensities given by Nahon *et al.* [46] for atomic bromine after the $3d^{-1}4p^6\,^2D_{5/2}$ transition, our data have been normalized so that line *H* ($3s^14p^5\ ^1P_1$) has the same intensity as that given in this reference, both measurements being made at the magic angle (54.7°). In some cases we have been able to separate lines that were unresolved by Nahon *et al.*, and in other cases these workers were unable to completely distinguish contributions from the two resonances. However, Table I indicates that the agreement is reasonable for all $3s^24p^4$ and $3s^14p^5$ lines and for those located in the kinetic-energy range 30–37 eV. There is a significant disagreement in the intensities for the $3s^03p^6$ line *Q*. This discrepancy probably arises from the problems with distinguishing contributions mentioned above.

The β values for the atomic lines, derived from their intensities at two pairs of angles (0° and 54.7°, 35.3°, and 90°), are shown in Table I as column 10 ($^2D_{5/2}$ resonance) and column 15 ($^2D_{3/2}$ resonance) and are plotted in Fig. 5. To the best of our knowledge this is the first time that such data have been obtained for HBr. From the table and the figure, one can see that the β values vary from −0.45 to 0.75, which again shows clearly that the anisotropy for some lines is large. Another feature one can note is that the β parameters for every *atomic line pair*, each of which decays to the same final HBr^+ state from one of the σ^* resonances, are similar. In fact, there are only two pairs for which the difference in β is larger than 0.1.

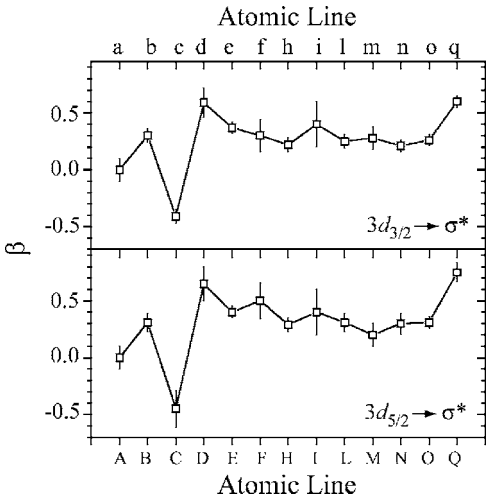

FIG. 5. Angular distribution parameters β for the atomic lines at the $^2D_{3/2}$ (upper panel) and $^2D_{5/2}$ (lower panel) resonances. Only the pairs of lines that are observed in both resonances in Fig. 2 are shown here. Note that the β values shown in this figure were derived using the line intensities determined after the molecular background has been subtracted.

E. Intrinsic anisotropy parameter α_2

As mentioned above, Sec. III D, the two-step nature of the core excitation of a molecule followed by dissociation and atomic Auger decay is reflected by expressing the asymmetry parameter β as a product of two factors [55,56]:

$$\beta = \alpha_2 \mathcal{A}_{20}, \tag{2}$$

where α_2 is the intrinsic anisotropy parameter in the Auger transition and $\mathcal{A}_{20}$ is the alignment parameter which reflects the anisotropy of the decaying state and, therefore, has the same value for all the transitions from that state. In the first approximation, following Ref. [55], the fourth-rank contribution $\alpha_4\mathcal{A}_{40}$ is neglected because of the small value of $\mathcal{A}_{40}$. The similarity in β values for the *atomic line pairs* mentioned above is surprising as the alignment parameters for the two resonance states are different [55]. Furthermore, the different values of the total angular momentum in the two resonance states means that the angular momentum carried away by the Auger electron may be different for decays from the $3d_{5/2} \rightarrow \sigma^*$ and $3d_{3/2} \rightarrow \sigma^*$ states to the same Br^+ state.

For transitions to final atomic states with $J=0$, there is only one outgoing partial wave and thus the α_2 value is fixed to be −1 for the $^2D_{5/2}$ resonance and −1.069 for the $^2D_{5/2}$ resonance [55]. Therefore, such states can be used to determine $\mathcal{A}_{20}$. In our HBr 2DPES, there are four lines corresponding to atomic ion states with zero total angular momentum for each resonance. Namely, $4s^24p^4\ ^3P_0$, which forms part of lines *B* and *b*; $4s^24p^4\,^1S_0$, lines *D* and *d*; $4s^14p^5\,^3P_0$,lines *G* and *g*; and $4s^04p^6\,^1S_0$, lines *Q* and *q*. The β associated with line *q* is the most reliable one, as all other lines either mix with their neighbors or sit on strong and

TABLE II. Anisotropy parameters α_2 evaluated from the Auger electron β parameters for the Br^* fragment following the photodissociation of HBr. These values are compared with those of the Auger lines in Kr.

Br*				Kr			
	Final state	Peak label	this work	Final state	Theory [57]	Experiment Ref.[58]	Experiment Ref.[47]
$Br^+_{5/2}$	$4s^24p^4(^3P_2)$	A	0.00(28)	$M_5N_{2,3}N_{2,3}(^3P_2)$	-0.329	-0.31(6)	
	$(^3P_1)$	B	-0.48(25)	$(^3P_1)$	-0.737		
	$(^3P_0)$	B	-0.48(25)	$(^3P_0)$	-1.069		
	$(^1D_2)$	C	0.70(38)	$(^1D_2)$	0.419	0.18(4)	
	$(^1S_0)$	D	-1.02(36)	$(^1S_0)$	-1.069		
	$4s^14p^5(^3P_2)$	E	-0.63(20)	$M_5N_1N_{2,3}(^3P_2)$	-0.746		-0.96(7)
	$(^3P_1)$	F	-0.78(38)	$(^3P_1)$	-1.011		-1.20(5)
	$(^3P_0)$	G	-1.03(52)	$(^3P_0)$	-1.069		-1.04(13)
	$(^1P_1)$	H	-0.45(22)	$(^1D_2)$	-0.569		-0.72(4)
	$4s^24p^3(^2P^0)5s(^1P_1)$	I	-0.63(44)				
	$4s^24p^3(^4S^0)5d(^3D)$	J	-				
	(^5D)	J	-				
	$4s^24p^3(^2P^0)5p(^3D)$	K	-0.78(44)				
	?	L	-0.48(25)				
	$4s^24p^3(^2D^0)5d(^1D)$	M	-0.31(28)				
	$4s^24p^3(^2D^0)4f(^1D)$	N	-0.47(27)				
	(^3F)	N	-0.47(27)				
	(^3D)	N	-0.47(27)				
	(^1F)	N	-0.47(27)				
	?	O	-0.48(20)				
	?	P	-				
	$4s^04p^6(^1S_0)$	Q	-1.17(25)	$M_5N_1N_1(^1S_0)$	-1.069		
$Br^+_{3/2}$	$4s^24p^4(^3P_2)$	a	0.00(25)	$M_4N_{2,3}N_{2,3}(^3P_2)$	0.095	0.21(9)	
	$(^3P_1)$	b	-0.50(18)	$(^3P_1)$	-0.818	-0.77(10)	
	$(^3P_0)$	b	-0.50(18)	$(^3P_0)$	-1.000	-0.77(10)	
	$(^1D_2)$	c	0.68(18)	$(^1D_2)$	0.224		
	$(^1S_0)$	d	-0.98(30)	$(^1S_0)$	-1.000		
	$4s^14p^5(^3P_2)$	e	-0.62(17)	$M_4N_1N_{2,3}(^3P_2)$	-0.839		-1.02(7)
	$(^3P_1)$	f	-0.50(32)	$(^3P_1)$	-0.895		-1.08(7)
	$(^3P_0)$	g	-	$(^3P_0)$	-1.000		
	$(^1P_1)$	h	-0.37(18)	$(^1P_1)$	-0.589		-0.77(4)
	$4s^24p^3(^2P^0)5s(^1P_1)$	i	-0.67(42)				
	$4s^24p^3(^4S^0)5d(^3D)$	j	-0.50(42)				
	(^5D)	j	-0.50(42)				
	$4s^24p^3(^2P^0)5p(^3D)$	k	-				
	?	l	-0.42(18)				
	$4s^24p^3(^2D^0)5d(^1D)$	m	-0.47(25)				
	$4s^24p^3(^2D^0)4f(^1D)$	n	-0.35(17)				
	(^3F)	n	-0.35(17)				
	(^3D)	n	-0.35(17)				
	(^1F)	n	-0.35(17)				
	?	o	-0.43(17)				
	?	p	-				
	$4s^04p^6(^1S_0)$	q	-1.00(17)	$M_4N_1N_1(^1S_0)$	-1.000		

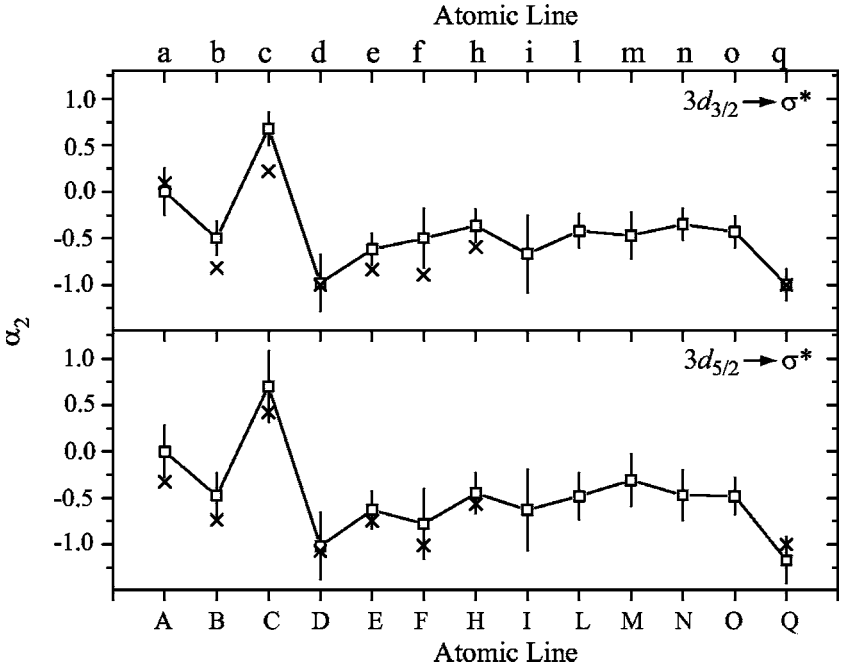

FIG. 6. Comparison of the intrinsic angular anisotropy parameters α_2 of the atomic lines in HBr with their corresponding normal Auger lines in Kr. Only the lines that are observed in both resonances in Fig. 2 are shown. In both panels, the open squares with error bars and connected with lines represent the α_2 values obtained in this work. The scattered crosses represent the theoretical calculations for Kr from Ref. [57]. For the correspondence between the lines in HBr and Kr, see Table II. Note that the β values, used to calculate the α_2 values shown in this figure, were derived using the line intensities determined after the molecular background has been subtracted.

variable molecular backgrounds. The β value of 0.60(5) for line q gives us $\mathcal{A}_{20}(^2D_{3/2})=-0.60(5)$, where the error bar results from the error on the β value.

From the relation between the alignment parameters of the two σ^* resonances in HBr [56],

$$\mathcal{A}_{20}(^2D_{5/2}) = \sqrt{8/7}\mathcal{A}_{20}(^2D_{3/2}), \tag{3}$$

we can obtain $\mathcal{A}_{20}(^2D_{5/2})=-0.64(5)$. This value is in reasonable agreement with the theoretical value of −0.74 given in Ref. [56]. The difference may be due to incomplete separation of the atomic lines from their molecular background on the experimental side or overestimation of the fragment alignment on the theoretical side. The experimental alignment parameter determined for $2p \rightarrow \sigma^*$ excitation in HCl is also lower than the theoretical prediction [56]. Using these two values for $\mathcal{A}_{20}$ and our β values listed in Table I, we can determine the anisotropy parameters α_2 for all other atomic lines which are listed in Table II and plotted in Fig. 6 as open squares.

The Br^* $(3d^{-1}4s^24p^6)$ core-excited state is isoelectronic with the $3d^{-1}$ core-hole state of Kr^+ and the atomic resonant Auger lines in Br have the same initial and final states as those in the normal Auger spectrum of krypton. Thus, it is reasonable to expect that the anisotropy parameters for the two sets of lines would be similar. A comparison between our data and the calculated values for α_2 of the $M_{4,5}N_1N_1$, $M_{4,5}N_1N_{2,3}$, and $M_{4,5}N_{2,3}$ Auger lines in Kr [57] is shown in Table II and plotted in Fig. 6. It is apparent that the two sets of values are similar, especially for the Br lines originating with the $3d_{5/2} \rightarrow \sigma^*$ resonance. However, our data do not agree well with the experimental Kr α_2 parameters [47,58] which are shown as the last two columns in Table II. For most lines, thedifference is larger than 0.3 units. It should be noted that there is also considerable discrepancy between the experimental and theoretical values in Kr, indicating that more effort is required in this area on both the theoretical and experimental sides.

IV. CONCLUSION

A detailed angle-resolved investigation of HBr including all the $3d$ resonances has been carried out using the technique of two-dimensional photoelectron spectroscopy. The two $3d^{-1}_{5/2,3/2}\sigma^*$ resonance peaks are resolved and found to be at photon energies of 70.89(6) eV and 71.92(6) eV, respectively. Some atomic Auger lines have been separated, and tentative assignments have been presented based on their kinetic-energy positions. We find that the profiles of the atomic Auger lines on the photon-energy, scale are not symmetric. The dissociation rate is known to increase with increasing photon energy, and the shape of the σ^* potential energy curves in the Frank-Condon region could also contribute to the asymmetry. The angular distributions of the atomic Auger decay lines at the two resonances have been analyzed. The atomic line pairs, corresponding to the decay of each resonance to the same final Br^+ state, have approximately the same angular distribution parameters, β. The alignment parameters $\mathcal{A}_{20}$ for the two resonances $3d^{-1}_{5/2,3/2}\sigma^*$ were found to be −0.64(5) $(^2D_{5/2})$ and −0.60(5) $(^2D_{3/2})$, respectively. The former is in reasonable agreement with the theoretical value of −0.74 predicted for the $^2D_{5/2}$ resonance. The intrinsic anisotropy parameters α_2 of the atomic lines have been derived using the appropriate β values and alignment parameters. The α_2 values were found to be similar to those calculated for the equivalent Auger lines in krypton.

ACKNOWLEDGMENTS

This work was supported by the Chemical Sciences, Geosciences and Biosciences Division, Office of Basic Energy

Sciences, Office of Science, U.S. Department of Energy under Contract No. DE-FG02-92ER14299. E.S. is grateful to Enterprise Ireland's International Collaboration Program for supporting the collaboration. X.F. thanks Dr. Thomas Gorzyca and Dr. Jun Fu for helpful discussions. We would also like to thank the staff at the ALS, especially John Bozek, Bruce Rude, and Sophie Canton, for their assistance.

[1] P. Morin and I. Nenner, Phys. Rev. Lett. **56**, 1913 (1986).
[2] A. Baev, P. Salek, F. K. Gel'mukhanov, H. Ågren, A. N. de Brito, O. Björneholm, and S. Svensson, Chem. Phys. **289**, 51 (2003).
[3] H. Aksela, S. Aksela, M. Ala-Korpela, O. -P. Sairanen, M. Hotokka, G. M. Bancroft, K. H. Tan, and J. Tulkki, Phys. Rev. A **41**, 6000 (1990).
[4] H. Aksela, S. Aksela, H. Hotokka, A. Yagishita, and E. Shigemasa, J. Phys. B **25**, 3357 (1992).
[5] U. Becker and A. Menzel, Nucl. Instrum. Methods Phys. Res. B **99**, 68 (1995).
[6] U. Hergenhahn and U. Becker, J. Electron Spectrosc. Relat. Phenom. **72**, 243 (1995).
[7] E. Kukk, H. Aksela, O. P. Sairanen, S. Aksela, A. Kivimäki, and E. Nõmmiste, J. Chem. Phys. **104**, 4475 (1996).
[8] O. Björneholm, S. Sundin, S. Svensson, R. R. T. Marinho, A. Naves de Brito, F. Gel'muukhanov, and H. Ågren, Phys. Rev. Lett. **79**, 3150 (1997).
[9] E. Kukk, A. Wills, N. Berrah, B. Langer, J. D. Bozek, O. Nayadin, M. Alsherhi, A. Farhat, and D. Cubaynes, Phys. Rev. A **57**, R1485 (1998), and references therein.
[10] A. Kivimäki, E. Kukk, J. Karvonen, J. Mursu, E. Nõmmiste, H. Aksela, and S. Aksela, Phys. Rev. A **57**, 2724 (1998).
[11] D. L. Hansen *et al.*, Phys. Rev. A **57**, 2608 (1998).
[12] Z. W. Gortel, R. Teshima, and D. Menzel, Phys. Rev. A **60**, 2159 (1999).
[13] R. Feifel *et al.*, Phys. Rev. Lett. **85**, 3133 (2000).
[14] A. Menzel, B. Langer, J. Viefhaus, S. B. Whitfield, and U. Becker, Chem. Phys. Lett. **258**, 265 (1996), and references therein.
[15] M. Meyer, S. Aloise, and A. N. Grum-Grzhimailo, Phys. Rev. Lett. **88**, 223001 (2002).
[16] Z. F. Liu, G. M. Bancroft, K. H. Tan, and M. Schachter, Phys. Rev. A **48**, R4019 (1993).
[17] I. Hjelte, M. N. Piancastelli, C. M. Jansson, K. Wiesner, O. Björneholm, M. Bössler, S. L. Sorensen, and S. Svensson, Chem. Phys. Lett. **370**, 781 (2003).
[18] K. Ueda, Y. Muramatsu, H. Chiba, Y. Sato, and E. Shigemasa, J. Electron Spectrosc. Relat. Phenom. **88-91**, 53 (1998).
[19] K. Ueda, J. Electron Spectrosc. Relat. Phenom. **88-91**, 1 (2000).
[20] I. Hjelte *et al.*, Chem. Phys. Lett. **334**, 151 (2001).
[21] H. Aksela, S. Aksela, A. Naves de Brito, G. M. Bancroft, and K. H. Tan, Phys. Rev. A **45**, 7948 (1992).
[22] A. Naves de Brito and H. Ågren, Phys. Rev. A **45**, 7953 (1992).
[23] B. Langer, A. Farhat, B. Nessar, N. Berrah, O. Hemmers, and J. D. Bozek (unpublished).
[24] N. Berrah, B. Langer, A. A. Wills, E. Kukk, J. D. Bozek, A. Farhat, and T. W. Gorczyca, J. Electron Spectrosc. Relat. Phenom. **101**, 1 (1999).
[25] A. A. Wills, E. Sokell, T. W. Gorczyca, X. Feng, M. Wiedenhoeft, S. E. Canton, and N. Berrah, J. Phys. B **35**, L367 (2002).
[26] A. Farhat, M. Humphrey, B. Langer, N. Berrah, J. D. Bozek, and D. Cubaynes, Phys. Rev. A **56**, 501 (1997).
[27] B. Langer, N. Berrah, A. Farhat, O. Hemmers, and J. D. Bozek, Phys. Rev. A **53**, R1946 (1996).
[28] X. Feng, Ph.D. thesis, Western Michigan University, 2005.
[29] C. E. Moore, *Atomic Energy Levels*, Natl. Bur. Stand. (U.S.) Circ. (U.S. Washington, D.C., 1971).
[30] J. Johnson, J. N. Cutler, G. M. Bancroft, Y. F. Hu, and K. H. Tan, J. Phys. B **30**, 4899 (1997).
[31] J. M. Bizau and F. Wuilleumier, J. Electron Spectrosc. Relat. Phenom. **71**, 205 (1995).
[32] F. Wuilleumier and M. O. Krause, J. Electron Spectrosc. Relat. Phenom. **15**, 15 (1979).
[33] R. Hentges, N. Müller, J. Viefhaus, U. Heinzmann, and U. Becker, J. Phys. B **37**, L267 (2004).
[34] X. Feng, A. A. Wills, E. Sokell, T. W. Gorczyca, M. Wiedenhoeft, and N. Berrah, Phys. Rev. A **72**, 042712 (2005).
[35] D. Čubrić, A. A. Wills, J. Comer, and M. A. MacDonald, J. Phys. B **25**, 5069 (1992).
[36] D. Čubrić, A. A. Wills, E. Sokell, J. Comer, and M. A. MacDonald, J. Phys. B **26**, 4425 (1993).
[37] E. Sokell, A. A. Wills, M. Wiedenhoft, X. Feng, D. Rolles, and N. Berrah, J. Phys. B **38**, 1535 (2005).
[38] A. J. Yencha, A. J. Cormach, R. J. Donovan, K. P. Lawley, A. Hopkirk, and G. C. King, Chem. Phys. **238**, 133 (1998).
[39] Y. F. Hu, G. M. Bancroft, J. Karvonen, E. Nommiste, A. Kivimaki, H. Aksela, S. Aksela, and Z. F. Liu, Phys. Rev. A **56**, R3342 (1997).
[40] R. Püttner, M. Domke, K. Schulz, A. Gutiérrez, and G. Kaindl, J. Phys. B **28**, 2425 (1995).
[41] Z. F. Liu, G. M. Bancroft, K. H. Tan, and M. Schachter, Phys. Rev. Lett. **72**, 621 (1994).
[42] B. Wannberg, S. Svensson, M. P. Keane, L. Karlsson, and P. Baltzer, Chem. Phys. **133**, 281 (1989).
[43] Z. F. Liu, G. M. Bancroft, K. H. Tan, and M. Schachter, J. Electron Spectrosc. Relat. Phenom. **67**, 299 (1994).
[44] R. Püttner, Y. F. Hu, G. M. Bancroft, H. Aksela, E. Nõmmiste, J. Karvonen, A. Kivimäki, and S. Aksela, Phys. Rev. A **59**, 4438 (1999).
[45] R. L. Kelly, J. Phys. Chem. Ref. Data **16** (1987), Suppl. 1.
[46] L. Nahon, P. Morin, and F. Combet-Farnoux, Phys. Scr. T **41**, 104 (1992).
[47] B. Kämmerling, B. Krässig, O. Schwarzkopf, J. P. Ribeiro, and V. Schmidt, J. Phys. B **25**, L5 (1992).
[48] J. Jauhiainen, H. Aksela, S. Aksela, A. Kivimäki, O. P. Sairanen, E. Nõmmiste, and J. Végh, J. Phys. B **3831**, R3342 (1995).
[49] C. E. Moore, *Atomic Energy Levels*, Natl. Bur. Stand. (U.S.)

Circ. No. 467 (U.S. GPO, Washington, D.C., 1958).
[50] E. J. McGuire, Phys. Rev. A **11**, 17 (1975).
[51] D. A. Shaw, D. Cvejanović, G. C. King, and F. H. Read, J. Phys. B **17**, 1173 (1984).
[52] A. P. Hitchcock and C. E. Brion, J. Electron Spectrosc. Relat. Phenom. **13**, 193 (1978).
[53] A. P. Hitchcock, M. Pocock, C. E. Brion, M. S. Banna, D. C. Frost, C. A. McDowell, and B. Wallbank, J. Electron Spectrosc. Relat. Phenom. **13**, 345 (1978).
[54] N. M. Kabachnik and I. P. Sazhina, J. Phys. B **17**, 1335 (1984).
[55] N. M. Kabachnik and I. P. Sazhina, J. Phys. B **21**, 267 (1988).
[56] N. M. Kabachnik, K. Ueda, Y. Muramatsu, and Y. Sato, J. Phys. B **31**, 4791 (1998).
[57] J. Tulkki, N. M. Kabachnik, and H. Aksela, Phys. Rev. A **48**, 1277 (1993).
[58] B. Kämmerling, V. Schmidt, W. Mehlhorn, W. B. Peatman, F. Schaefers, and T. Schroeter, J. Phys. B **22**, L597 (1989).